Importance line sampling for first excursion probability and sensitivity estimation in linear systems under Gaussian loading

M.A. Misraji [1], **M.A. Valdebenito** [1], **C. Papadimitriou** [2], **M.G.R. Faes** [1,3]
[1] TU Dortmund University, Chair for Reliability Engineering,
Dortmund 44227, Germany

[2] University of Thessaly, Department of Mechanical Engineering,
Volos 38221, Greece

[3] Tongji University, International Joint Research Center for Engineering Reliability and Stochastic Mechanics,
Shanghai 200092, China
e-mail: **mauricio.misraji@tu-dortmund.de**

Abstract
This work introduces the Importance Line Sampling technique for estimating the first excursion probability and its sensitivity in linear dynamical systems subject to Gaussian loading. The method exploits the linear dependence of the structural response on the Gaussian input variables. This relationship induces a failure domain with a special structure, defined as the union of elementary failure domains in a high-dimensional standard Gaussian space. The proposed estimator is based on Line Sampling and combines multiple coordinate-system definitions with an importance sampling density, both constructed from the geometry of the elementary failure domains. The failure probability is evaluated by analytical line integration, and its gradient is obtained as a byproduct of the first excursion probability estimation. The efficiency of the approach for estimating both the failure probability and its sensitivity is demonstrated through a large-scale finite element model.

1 Introduction

The reliability assessment of structural systems subjected to stochastic dynamic loading is of utmost importance in engineering design. In this context, uncertain effects such as wind, earthquake excitation, vibrations, or impact-type loads can be described more realistically through stochastic models than with purely deterministic representations. As a consequence, the system response also becomes stochastic and has to be characterized by suitable probabilistic measures. In stochastic dynamics, the so-called first excursion probability is particularly relevant, since it quantifies the probability that one or more responses of interest exceed prescribed threshold levels within the duration of the excitation [1, 2, 3]. This measure is well suited for serviceability-oriented analyses, where the response levels of interest are commonly associated with linear structural behavior [4, 5].

The estimation of first excursion probabilities is a challenging task, since the stochastic excitation is typically represented by a large number of random variables, leading to a high-dimensional probability integral. For linear systems under Gaussian loading, this difficulty can be partly reduced by exploiting the special geometry of the failure domain within dedicated simulation schemes. After time discretization, each threshold exceedance associated with a response component and a time instant defines an elementary failure domain in the standard Gaussian space. Since the response depends linearly on the Gaussian vector, each elementary failure domain is bounded by a hyperplane. Accordingly, the overall failure domain is obtained as the union

of all elementary failure domains, whose analytical definition provides the geometric information used to guide the simulation procedure. This idea has been leveraged by several methods, including Efficient Importance Sampling [6], the Domain Decomposition Method (DDM) [7], Directional Importance Sampling (DIS) [8], and multidomain Line Sampling (mLS) [9].

In many applications, the first excursion probability alone is not sufficient, since changes in structural parameters may significantly affect the reliability of the system. Therefore, its gradient provides useful information for several applications, including, for example, model updating, reliability-based design optimization, and risk-informed decision making [10, 11, 12, 13]. In this work, the sensitivities are local and are evaluated with respect to deterministic design parameters, such as masses, stiffness coefficients, geometric dimensions, or material properties. Existing sensitivity estimators for first excursion probabilities are commonly constructed as a post-processing step of a reliability analysis. Directional approaches such as DIS and DDM can provide both quantities by exploring one-dimensional rays anchored at the origin and by incorporating importance sampling densities constructed from the elementary failure-domain information [14, 7]. In these methods, the failure domain is approached radially from the origin, and the contribution along each sampled ray is evaluated by exploiting the linear structure of the elementary domains. Line Sampling methods, on the other hand, explore lines that are not necessarily constrained to pass through the origin. This alternative placement of the explored lines can be advantageous when the relevant parts of the limit-state boundary are reached more effectively by lines aligned with suitable important directions [15, 16]. This motivates the combination of line-wise exploration with an importance sampling density, leading to the formulation presented in this work.

In this contribution, Importance Line Sampling (ILS) is developed as a simulation framework for estimating the first excursion probability and its sensitivity in linear dynamical systems subject to Gaussian loading. The approach combines a multiple-coordinate-system Line Sampling representation with an importance sampling density constructed from the elementary failure-domain information. The resulting estimator evaluates the first excursion probability by analytical line integration, while the sensitivity estimate is obtained as a byproduct of the same simulation procedure. The approach is illustrated with a large-scale finite element model of a curved bridge, and its efficiency is compared with existing methods from the literature.

The remainder of the paper is organized as follows. Section 2 defines the class of problems considered and the corresponding sensitivity measure. Section 3 presents the proposed ILS formulation. Section 4 illustrates the method with a large-scale finite element model. Finally, Section 5 summarizes the main ideas and outlines future developments.

2 Problem statement

2.1 Gaussian loading

The excitation is described over the time interval $[0, T]$ at the discrete time instants $t_k = (k-1)\Delta t$, $k = 1, \ldots, n_T$, where n_T denotes the total number of time instants. Its stochastic character is represented by a finite-dimensional Karhunen–Loève expansion [1]:

$$p(t_k, \boldsymbol{z}) = \mu_k + \boldsymbol{\psi}_k^{\mathrm{T}} \boldsymbol{z}, \qquad k = 1, \ldots, n_T, \tag{1}$$

where $\boldsymbol{z}$ is a realization of the standard Gaussian random vector $\boldsymbol{Z} \in \mathbb{R}^{n_{KL}}$, n_{KL} denotes the truncation order, $\boldsymbol{\psi}_k \in \mathbb{R}^{n_{KL}}$ is the Karhunen–Loève vector associated with t_k, and μ_k is the mean value of the excitation at t_k. In this work, the excitation is assumed to have zero mean for simplicity.

2.2 Structural system

The structural system is assumed to be linear with proportional damping, and its properties depend on the parameter vector $\boldsymbol{y} \in \mathbb{R}^{n_Y}$, where $\boldsymbol{y}$ collects the deterministic design parameters, with n_Y denoting the

dimension of this parameter vector. Then, the equation of motion is written as [17]

$$\boldsymbol{M}(\boldsymbol{y})\ddot{\boldsymbol{x}}(t,\boldsymbol{y},\boldsymbol{z}) + \boldsymbol{C}(\boldsymbol{y})\dot{\boldsymbol{x}}(t,\boldsymbol{y},\boldsymbol{z}) + \boldsymbol{K}(\boldsymbol{y})\boldsymbol{x}(t,\boldsymbol{y},\boldsymbol{z}) = \boldsymbol{g}_c(\boldsymbol{y})p(t,\boldsymbol{z}), \qquad t \in [0,T], \tag{2}$$

where $\boldsymbol{x}$, $\dot{\boldsymbol{x}}$, and $\ddot{\boldsymbol{x}}$ denote the displacement, velocity, and acceleration vectors. The matrices $\boldsymbol{M}$, $\boldsymbol{C}$, and $\boldsymbol{K}$ define the mass, damping, and stiffness properties of the system, whereas $\boldsymbol{g}_c$ is the load-coupling vector associated with the scalar excitation $p(t,\boldsymbol{z})$.

The responses of interest are denoted by $\eta_i(t,\boldsymbol{y},\boldsymbol{z})$, $i = 1,\ldots,n_\eta$, where n_η is the total number of responses considered in the analysis. Owing to linearity, each response can be evaluated by convolution of the excitation with the corresponding unit impulse response function [17]:

$$\eta_i(t,\boldsymbol{y},\boldsymbol{z}) = \int_0^t h_i(t-\tau,\boldsymbol{y})p(\tau,\boldsymbol{z})\,d\tau, \qquad i = 1,\ldots,n_\eta. \tag{3}$$

where $h_i(t,\boldsymbol{y})$ denotes the unit impulse response function associated with the i-th response of interest. After time discretization, the Gaussian representation in Eq. (1) allows the responses to be written as linear functions of the Gaussian input variables:

$$\eta_i(t_k,\boldsymbol{y},\boldsymbol{z}) = \boldsymbol{a}_{i,k}(\boldsymbol{y})^{\mathrm{T}}\boldsymbol{z}, \qquad i = 1,\ldots,n_\eta, \quad k = 1,\ldots,n_T, \tag{4}$$

where the vector $\boldsymbol{a}_{i,k}(\boldsymbol{y}) \in \mathbb{R}^{n_{KL}}$ is obtained from the unit impulse response function $h_i(t,\boldsymbol{y})$ associated with the i-th response of interest:

$$\boldsymbol{a}_{i,k}(\boldsymbol{y}) = \sum_{m=1}^{k} \Delta t\,\epsilon_m h_i(t_k - t_m,\boldsymbol{y})\boldsymbol{\psi}_m. \tag{5}$$

In Eq. (5), ϵ_m contains the weights associated with the numerical integration rule used to approximate the convolution integral. For the trapezoidal rule, $\epsilon_m = 1/2$ for $m = 1$ or $m = k$, and $\epsilon_m = 1$ for the remaining points. In this representation of the response of interest, the dependence on the Gaussian input variables appears through $\boldsymbol{z}$, while the dependence on the deterministic parameters is contained in $\boldsymbol{a}_{i,k}(\boldsymbol{y})$.

2.3 First excursion probability

The threshold levels assigned to the responses of interest are collected in $\boldsymbol{b} \in \mathbb{R}^{n_\eta}$, with b_i denoting the prescribed limit for the i-th response. A first excursion takes place when at least one response exceeds its corresponding threshold during the excitation interval. This event is described by the performance function

$$g(\boldsymbol{y},\boldsymbol{z}) = 1 - \max_{i=1,\ldots,n_\eta}\left(\max_{k=1,\ldots,n_T}\frac{|\eta_i(t_k,\boldsymbol{y},\boldsymbol{z})|}{b_i}\right). \tag{6}$$

Accordingly, realizations satisfying $g(\boldsymbol{y},\boldsymbol{z}) \le 0$ belong to the failure domain, which is defined in the standard Gaussian space as

$$F = \{\boldsymbol{z} \in \mathbb{R}^{n_{KL}} : g(\boldsymbol{y},\boldsymbol{z}) \le 0\}. \tag{7}$$

The probability of this event is quantified by the first excursion probability [1]:

$$p_F(\boldsymbol{y}) = \int_{\mathbb{R}^{n_{KL}}} I_F(\boldsymbol{y},\boldsymbol{z}) f_{\boldsymbol{Z}}(\boldsymbol{z})\,d\boldsymbol{z}, \tag{8}$$

where $I_F(\boldsymbol{y},\boldsymbol{z})$ denotes the indicator of the failure domain F, and $f_{\boldsymbol{Z}}$ is the standard Gaussian probability density function. Since the stochastic excitation is represented by n_{KL} Gaussian variables, Eq. (8) generally defines a high-dimensional probability integral. For the applications considered here, this integral is not available in closed form and is therefore estimated by simulation. The geometric structure induced by Eq. (6), together with the linear representation in Eq. (4), is discussed in the next subsection.

2.4 Geometry of the failure domain

The linear response representation in Eq. (4) provides an analytical description of the failure domain in the standard Gaussian space. For each response of interest η_i and each time instant t_k, exceedance of the threshold in either direction defines an elementary failure domain [18]. Its positive and negative parts are given by

$$F_{i,k}^{+} = \left\{ \boldsymbol{z} \in \mathbb{R}^{n_{KL}} : \boldsymbol{a}_{i,k}(\boldsymbol{y})^{\mathrm{T}} \boldsymbol{z} \geq b_i \right\}, \qquad F_{i,k}^{-} = \left\{ \boldsymbol{z} \in \mathbb{R}^{n_{KL}} : \boldsymbol{a}_{i,k}(\boldsymbol{y})^{\mathrm{T}} \boldsymbol{z} \leq -b_i \right\}. \tag{9}$$

Accordingly, the elementary failure domain associated with the pair (i, k) is defined as

$$F_{i,k} = F_{i,k}^{+} \cup F_{i,k}^{-}. \tag{10}$$

Since the failure domain in Eq. (7) corresponds to the occurrence of at least one elementary failure event, it can be written as the union of all elementary failure domains:

$$F = \bigcup_{i=1}^{n_\eta} \bigcup_{k=1}^{n_T} F_{i,k}. \tag{11}$$

This decomposition shows that the geometry is governed by $n_\eta n_T$ elementary failure domains. Each of them is bounded by a hyperplane and may overlap with other elementary domains. Figure 1 illustrates this structure for the case $n_\eta = 1$ and $n_T = n_{KL} = 2$. In this two-dimensional setting, the elementary limit-state functions $g_{1,k}^{+}$ and $g_{1,k}^{-}$, with $k = 1, 2$, define the boundaries of the positive and negative elementary failure domains $F_{1,k}^{+}$ and $F_{1,k}^{-}$, respectively. The associated design points $\boldsymbol{z}_{1,k}^{*}(\boldsymbol{y})$ and $-\boldsymbol{z}_{1,k}^{*}(\boldsymbol{y})$ are also shown for $k = 1, 2$. Note that some regions belong to more than one elementary failure domain. Physically, this means that the same realization of the stochastic excitation can produce threshold exceedance of the same response at more than one time instant, although the corresponding first excursion event is counted only once.

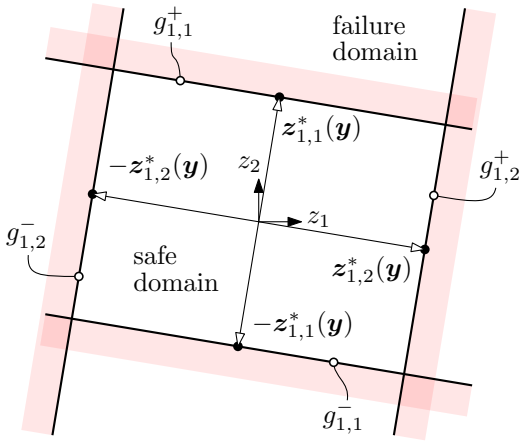

Figure 1: Schematic representation of the elementary failure domains in the standard Gaussian space.

The design point associated with the positive elementary failure domain $F_{i,k}^{+}$ is the point on its boundary with minimum Euclidean norm. It is defined as

$$\boldsymbol{z}_{i,k}^{*}(\boldsymbol{y}) = b_i \frac{\boldsymbol{a}_{i,k}(\boldsymbol{y})}{\|\boldsymbol{a}_{i,k}(\boldsymbol{y})\|^2}, \qquad \beta_{i,k}(\boldsymbol{y}) = \frac{b_i}{\|\boldsymbol{a}_{i,k}(\boldsymbol{y})\|}. \tag{12}$$

Here, $\|\cdot\|$ denotes the Euclidean norm and $\beta_{i,k}(\boldsymbol{y})$ is the corresponding reliability index. The design point associated with $F_{i,k}^{-}$ is obtained analogously with opposite sign. Since the elementary limit-state functions are linear in the Gaussian space, the probability of occurrence of each elementary failure domain can be written as

$$P\left[F_{i,k}\right] = P\left[F_{i,k}^{+}\right] + P\left[F_{i,k}^{-}\right] = 2\Phi\left(-\beta_{i,k}\right), \tag{13}$$

where $\Phi(\cdot)$ denotes the cumulative distribution function of a standard Gaussian random variable.

2.5 Gradient of the failure probability

The sensitivity of the first excursion probability with respect to a deterministic design parameter y_q is defined through the gradient component $\partial p_F(\boldsymbol{y})/\partial y_q$. For the reliability problem defined above, differentiating the first excursion probability with respect to y_q leads to a surface integral over the limit-state hypersurface [13]:

$$\frac{\partial p_F(\boldsymbol{y})}{\partial y_q} = -\int_{g(\boldsymbol{y},\boldsymbol{z})=0} \frac{\partial g(\boldsymbol{y},\boldsymbol{z})}{\partial y_q} \frac{1}{\|\nabla_{\boldsymbol{z}} g(\boldsymbol{y},\boldsymbol{z})\|} f_{\boldsymbol{Z}}(\boldsymbol{z})\, dS, \qquad q = 1,\dots,n_Y, \tag{14}$$

where $\partial(\cdot)/\partial y_q$ denotes partial differentiation with respect to the q-th deterministic parameter, $\nabla_{\boldsymbol{z}}$ denotes the gradient operator with respect to the Gaussian vector $\boldsymbol{z}$, and dS is a differential element of the limit-state hypersurface. The direct evaluation of Eq. (14) is difficult because it involves integration over a surface of dimension $n_{KL}-1$. Therefore, the sensitivity estimation is addressed in the following within the same simulation framework used for the reliability analysis.

3 Importance Line Sampling

This section presents the proposed Importance Line Sampling formulation. The multiple-coordinate-system representation is introduced in Section 3.1, where coordinate systems associated with the elementary failure domains are defined. The explored lines and the line-wise quantities required to evaluate the failure-domain contribution are then introduced in Section 3.2, followed by the construction of the importance sampling density in Section 3.3. Finally, the reliability and sensitivity estimators are presented in Sections 3.4 and 3.5, respectively, and the main implementation steps are summarized in Section 3.6.

3.1 Multiple-coordinate-system formulation

Classical Line Sampling evaluates a failure probability by introducing an important direction, which defines a rotated coordinate system in the standard Gaussian space. The failure domain is then explored by performing one-dimensional integrations along lines parallel to this direction [19]. Based on the decomposition in Eq. (11), ILS assigns one such coordinate system to each response–time pair (i,k). The directions of the design points defined in Eq. (12) are used to define these coordinate systems, whereas the elementary probabilities in Eq. (13) are later used to construct the importance sampling density. These coordinate systems are indexed by a single index $j = 1,\dots,n_c$, with $n_c = n_\eta n_T$. Thus, j is a compact enumeration of the elementary failure domains, and the corresponding elementary failure domain and design point are denoted by F_j and $\boldsymbol{z}_j^*(\boldsymbol{y})$, respectively. The important direction of the j-th coordinate system is defined from the corresponding design point, and any realization $\boldsymbol{z}$ can be expressed in this system as

$$\boldsymbol{\alpha}_j = \frac{\boldsymbol{z}_j^*(\boldsymbol{y})}{\|\boldsymbol{z}_j^*(\boldsymbol{y})\|}, \qquad \boldsymbol{z} = \boldsymbol{R}_j \boldsymbol{z}_j^{\perp} + z_j^{\parallel}\boldsymbol{\alpha}_j. \tag{15}$$

Here, $\boldsymbol{R}_j \in \mathbb{R}^{n_{KL}\times(n_{KL}-1)}$ contains an orthonormal basis of the hyperplane orthogonal to $\boldsymbol{\alpha}_j$, so that $z_j^{\parallel} \in \mathbb{R}$ and $\boldsymbol{z}_j^{\perp} \in \mathbb{R}^{n_{KL}-1}$ are the parallel and perpendicular coordinates of $\boldsymbol{z}$ in the j-th coordinate system, respectively. Since the transformation is orthonormal, the standard Gaussian measure is invariant under this rotation.

The same first excursion probability can be represented in any of the coordinate systems. ILS therefore uses a mixture representation:

$$p_F = \sum_{j=1}^{n_c} \rho_j p_F^j. \tag{16}$$

Here, p_F^j denotes the representation of the first excursion probability in the j-th coordinate system, and the weights ρ_j satisfy $\sum_{j=1}^{n_c} \rho_j = 1$.

Figure 2 illustrates the coordinate-system definitions for the case $n_\eta = 1$ and $n_T = n_{KL} = 3$. The same failure domain is shown in the three panels, but each panel uses a different coordinate system associated with one elementary failure domain. In the first panel, the parallel coordinate $z_1^{\parallel}$ is aligned with $\boldsymbol{\alpha}_1$, associated with $F_{1,1}$; in the second panel, $z_2^{\parallel}$ is aligned with $\boldsymbol{\alpha}_2$, associated with $F_{1,2}$; and in the third panel, $z_3^{\parallel}$ is aligned with $\boldsymbol{\alpha}_3$, associated with $F_{1,3}$. The corresponding perpendicular coordinates $\boldsymbol{z}_j^{\perp}$ span the hyperplane orthogonal to $\boldsymbol{\alpha}_j$. Therefore, for a fixed realization of $\boldsymbol{z}_j^{\perp}$, varying $z_j^{\parallel}$ defines a line parallel to $\boldsymbol{\alpha}_j$. Although the failure domain is unchanged, each coordinate system provides a different representation of the same first excursion event within the Line Sampling scheme, as made explicit through the line-wise quantities introduced next.

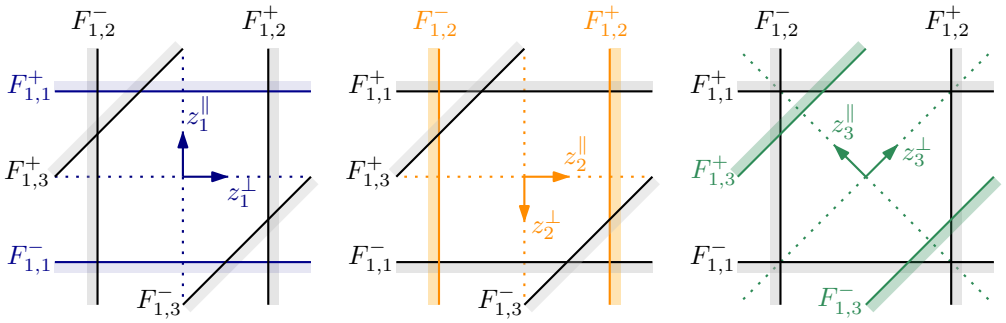

Figure 2: Coordinate-system definition used in the Importance Line Sampling formulation.

3.2 Line-wise quantities

For a fixed realization $\boldsymbol{z}_j^{\perp}$ in the j-th coordinate system, varying only the scalar coordinate $z_j^{\parallel}$ traces the explored line, namely $\ell_j(\boldsymbol{z}_j^{\perp}) = \{\boldsymbol{R}_j \boldsymbol{z}_j^{\perp} + z_j^{\parallel} \boldsymbol{\alpha}_j : z_j^{\parallel} \in \mathbb{R}\}$. For compactness, the notation ℓ_j is used generically, with the understanding that different realizations of $\boldsymbol{z}_j^{\perp}$ define different lines in the same coordinate system.

For a fixed line ℓ_j, the coordinate along the line is denoted by c, so that points on the line can be written as $\boldsymbol{z} = \boldsymbol{R}_j \boldsymbol{z}_j^{\perp} + c\boldsymbol{\alpha}_j$. Here, c is the signed distance measured in the direction $\boldsymbol{\alpha}_j$, and $f_{Z_j^{\parallel}}$ denotes the one-dimensional standard Gaussian probability density function associated with this coordinate. Along this line, each elementary failure domain defines an elementary safe interval in terms of c. The limits of these intervals are obtained directly from Eq. (4) by evaluating the response along the fixed line and solving the corresponding threshold equalities for c. The intersection of all these elementary safe intervals determines the safe segment of the complete failure domain. Its lower and upper bounds are denoted by $c_S^{L,j}$ and $c_S^{U,j}$, respectively, so that each fixed line ℓ_j is associated with a unique pair of bounds. If $c_S^{L,j} < c_S^{U,j}$, the line contains a finite safe segment and the exterior portions belong to the failure domain. If $c_S^{L,j} \geq c_S^{U,j}$, no common safe segment exists and the whole line is contained in the failure domain. For a fixed perpendicular realization $\boldsymbol{z}_j^{\perp}$, the line ℓ_j is fixed and only the coordinate $z_j^{\parallel}$ varies. Since this coordinate follows a standard Gaussian distribution, the probability content associated with the portion of ℓ_j lying in the complete failure domain is obtained by integrating $f_{Z_j^{\parallel}}$ over the corresponding failure intervals. This line-wise failure contribution is denoted by $A(\ell_j, \boldsymbol{y})$ and is defined as

$$A(\ell_j, \boldsymbol{y}) = \begin{cases} \displaystyle\int_{-\infty}^{\infty} f_{Z_j^{\parallel}}(c)\, dc = 1, & c_S^{L,j} \geq c_S^{U,j}, \\ \displaystyle\int_{-\infty}^{c_S^{L,j}} f_{Z_j^{\parallel}}(c)\, dc + \int_{c_S^{U,j}}^{\infty} f_{Z_j^{\parallel}}(c)\, dc = \Phi(c_S^{L,j}) + \Phi(-c_S^{U,j}), & c_S^{L,j} < c_S^{U,j}. \end{cases} \tag{17}$$

Note that the safe-segment bounds $c_S^{L,j}$ and $c_S^{U,j}$ depend on the design vector $\boldsymbol{y}$. To simplify the notation, this dependence is not shown explicitly in the bounds and is reflected only through the line-wise contribution $A(\ell_j, \boldsymbol{y})$. Figure 3 illustrates these line-wise quantities for the case $n_\eta = 1$ and $n_T = n_{KL} = 3$. The parenthetical superscript is used only to distinguish representative line realizations. For the line $\ell_3^{(1)}$, the elementary safe intervals have a common intersection, leading to the finite safe segment bounded by $c_S^{L,3}$ and $c_S^{U,3}$. The line-wise contribution $A(\ell_3^{(1)}, \boldsymbol{y})$ is then obtained from the two exterior failure portions of the line. For the line $\ell_1^{(2)}$, the elementary safe intervals do not overlap. Therefore, no finite safe segment exists and the whole line belongs to the failure domain, leading to $A(\ell_1^{(2)}, \boldsymbol{y}) = 1$.

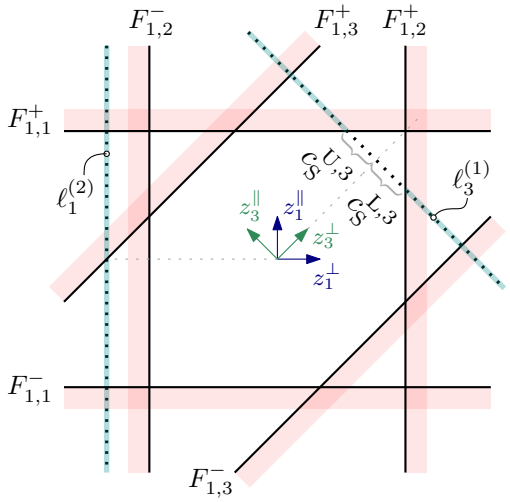

Figure 3: Line-wise representation of the failure event in the ILS formulation.

3.3 Importance sampling density

Following the elementary-domain construction used in importance sampling [6], the density is defined as a mixture of conditional densities associated with the elementary failure events. Since this density is formulated in the standard Gaussian space, it can be expressed in any of the rotated coordinate systems. In the j-th coordinate system, it is written as

$$f_{\boldsymbol{Z}}^{\mathrm{IS},j}(z_j^{\parallel}, \boldsymbol{z}_j^{\perp}) = f_{\boldsymbol{Z}_j^{\perp}}^{\mathrm{IS},j}(\boldsymbol{z}_j^{\perp}) f_{Z_j^{\parallel}}(z_j^{\parallel}) = \sum_{i=1}^{n_\eta} \sum_{k=1}^{n_T} \omega_{i,k} f_{\boldsymbol{Z}_j^{\perp}}(\boldsymbol{z}_j^{\perp} \mid F_{i,k}) f_{Z_j^{\parallel}}(z_j^{\parallel}), \tag{18}$$

where $f_{\boldsymbol{Z}_j^{\perp}}(\boldsymbol{z}_j^{\perp} \mid F_{i,k})$ is the density of the perpendicular component conditioned on the occurrence of the elementary failure event $F_{i,k}$. The mixture weights are chosen proportional to the elementary failure-domain probabilities [6]:

$$\omega_{i,k} = \frac{P[F_{i,k}]}{\sum_{h=1}^{n_\eta} \sum_{m=1}^{n_T} P[F_{h,m}]} = \frac{2\Phi(-\beta_{i,k})}{\sum_{h=1}^{n_\eta} \sum_{m=1}^{n_T} 2\Phi(-\beta_{h,m})}. \tag{19}$$

The denominator in Eq. (19) is denoted by $\hat{p}_F = \sum_{h=1}^{n_\eta} \sum_{m=1}^{n_T} P[F_{h,m}]$, which corresponds to the sum of the elementary probabilities considered independently and therefore provides an upper bound of the first excursion probability.

Although Eq. (18) is written in the j-th coordinate system, the density itself is not conditioned on j; the index only identifies the rotated representation used for the parallel–perpendicular decomposition. For a fixed realization $\boldsymbol{z}_j^{\perp}$, the conditional probability associated with each elementary failure event is expressed

through the corresponding elementary line-wise contribution. Therefore, the density ratio becomes

$$\frac{f_{\boldsymbol{Z}}(z_j^{\parallel}, \boldsymbol{z}_j^{\perp})}{f_{\boldsymbol{Z}}^{\mathrm{IS},j}(z_j^{\parallel}, \boldsymbol{z}_j^{\perp})} = \frac{\hat{p}_F}{A_{\Sigma}^{j}(\ell_j)}. \tag{20}$$

Here, $A_{\Sigma}^{j}(\ell_j, \boldsymbol{y})$ denotes the sum of the elementary line-wise contributions $A_{i,k}^{j}(\ell_j, \boldsymbol{y})$ associated with the line ℓ_j, namely

$$A_{\Sigma}^{j}(\ell_j, \boldsymbol{y}) = \sum_{i=1}^{n_\eta} \sum_{k=1}^{n_T} A_{i,k}^{j}(\ell_j, \boldsymbol{y}). \tag{21}$$

For compactness, the dependence on $\boldsymbol{y}$ is omitted in Eq. (20).

3.4 Reliability estimator

Starting from the first excursion probability in Eq. (8), the multiple-coordinate-system representation in Eq. (16) is used. Then, introducing the importance sampling density defined in Eq. (18), the failure probability integral can be written as

$$p_F(\boldsymbol{y}) = \sum_{j=1}^{n_c} \rho_j \int_{\mathbb{R}^{n_{KL}-1}} \int_{\mathbb{R}} I_F(\boldsymbol{y}, z_j^{\parallel}, \boldsymbol{z}_j^{\perp}) \frac{f_{\boldsymbol{Z}}(z_j^{\parallel}, \boldsymbol{z}_j^{\perp})}{f_{\boldsymbol{Z}}^{\mathrm{IS},j}(z_j^{\parallel}, \boldsymbol{z}_j^{\perp})} f_{\boldsymbol{Z}}^{\mathrm{IS},j}(z_j^{\parallel}, \boldsymbol{z}_j^{\perp})\, dz_j^{\parallel} d\boldsymbol{z}_j^{\perp}. \tag{22}$$

For a fixed realization $\boldsymbol{z}_j^{\perp}$, the explored line $\ell_j(\boldsymbol{z}_j^{\perp})$ is fixed and the density ratio in Eq. (20) does not depend on the parallel coordinate $z_j^{\parallel}$. Therefore, the inner integration along $z_j^{\parallel}$ can be evaluated analytically by means of the line-wise contribution $A(\ell_j)$ defined in Eq. (17), yielding

$$p_F(\boldsymbol{y}) = \sum_{j=1}^{n_c} \rho_j \int_{\mathbb{R}^{n_{KL}-1}} A\Big(\ell_j(\boldsymbol{z}_j^{\perp}), \boldsymbol{y}\Big) \frac{\hat{p}_F}{A_{\Sigma}^{j}\Big(\ell_j(\boldsymbol{z}_j^{\perp})\Big)} f_{\boldsymbol{Z}_j^{\perp}}^{\mathrm{IS},j}(\boldsymbol{z}_j^{\perp})\, d\boldsymbol{z}_j^{\perp}, \tag{23}$$

where $f_{\boldsymbol{Z}_j^{\perp}}^{\mathrm{IS},j}$ denotes the importance sampling density of the perpendicular coordinates in the j-th coordinate system. In Eq. (23), the dependence on $\boldsymbol{y}$ is shown explicitly only for the complete line-wise contribution A, since this quantity changes through the safe-segment bounds and it needs to be differentiated to obtain probability sensitivity (as shown in detail in Section 3.5). The quantities ρ_j, $\hat{p}_F$, $f_{\boldsymbol{Z}_j^{\perp}}^{\mathrm{IS},j}$, and A_{Σ}^{j} define the importance sampling density for the design under consideration. In the local sensitivity calculation, these quantities are kept fixed, and their dependence on $\boldsymbol{y}$ is therefore omitted from the notation.

The estimator is obtained by sampling N lines from the representation in Eq. (23). For convenience, the coordinate-system selection probabilities are chosen consistently with the mixture weights in Eq. (19). Thus, under the single-index correspondence $j \leftrightarrow (i,k)$, $\rho_j = \omega_{i,k}$. For the r-th sample, j_r denotes the selected coordinate-system index, and $\ell_{j_r,r}$ denotes the line generated in that coordinate system from the realization $\boldsymbol{z}_{j_r,r}^{\perp}$ sampled according to $f_{\boldsymbol{Z}_{j_r}^{\perp}}^{\mathrm{IS},j_r}$. Thus, the first subscript in $\ell_{j_r,r}$ identifies the coordinate system used for sample r, while the second subscript identifies the sample number. With this notation, $A(\ell_{j_r,r})$ and $A_{\Sigma}^{j_r}(\ell_{j_r,r})$ denote the evaluated line-wise quantities for the r-th simulated line, and Eq. (23) leads to the Importance Line Sampling estimator of the first excursion probability:

$$\tilde{p}_F = \frac{\hat{p}_F}{N} \sum_{r=1}^{N} \frac{A(\ell_{j_r,r})}{A_{\Sigma}^{j_r}(\ell_{j_r,r})}. \tag{24}$$

The statistical uncertainty of the estimator is quantified through its coefficient of variation, computed from

the sample variance of the line-wise contributions as

$$\delta_{\tilde{p}_F} = \frac{1}{\tilde{p}_F} \sqrt{\frac{1}{N(N-1)} \sum_{r=1}^{N} \left(\hat{p}_F \frac{A(\ell_{j_r,r})}{A_{\Sigma}^{j_r}(\ell_{j_r,r})} - \tilde{p}_F \right)^2}. \tag{25}$$

3.5 Sensitivity estimator

The sensitivity estimator is derived from the probability expression obtained after the analytical integration along the parallel coordinate. Using the line-wise contribution $A(\ell_j)$ defined in Eq. (17), the first excursion probability can be written as

$$p_F(\boldsymbol{y}) = \sum_{j=1}^{n_c} \rho_j \int_{\mathbb{R}^{n_{KL}-1}} A\Big(\ell_j(\boldsymbol{z}_j^{\perp}), \boldsymbol{y}\Big)\, f_{\boldsymbol{Z}_j^{\perp}}(\boldsymbol{z}_j^{\perp})\, d\boldsymbol{z}_j^{\perp}. \tag{26}$$

In the local calculation, the coordinate systems and the weights ρ_j are constructed for the design under consideration and kept fixed. Therefore, differentiating Eq. (26) with respect to y_q affects only the line-wise contribution $A(\ell_j, \boldsymbol{y})$, through the displacement of the active safe-segment bounds. The importance sampling density is then introduced for the resulting integral. Using the density ratio in Eq. (20), the gradient can be written as

$$\frac{\partial p_F(\boldsymbol{y})}{\partial y_q} = \hat{p}_F \sum_{j=1}^{n_c} \rho_j \int_{\mathbb{R}^{n_{KL}-1}} \frac{\partial A(\ell_j(\boldsymbol{z}_j^{\perp}), \boldsymbol{y})}{\partial y_q} \frac{f_{\boldsymbol{Z}_j^{\perp}}^{\mathrm{IS},j}(\boldsymbol{z}_j^{\perp})}{A_{\Sigma}^{j}(\ell_j(\boldsymbol{z}_j^{\perp}))}\, d\boldsymbol{z}_j^{\perp}, \qquad q = 1, \ldots, n_Y. \tag{27}$$

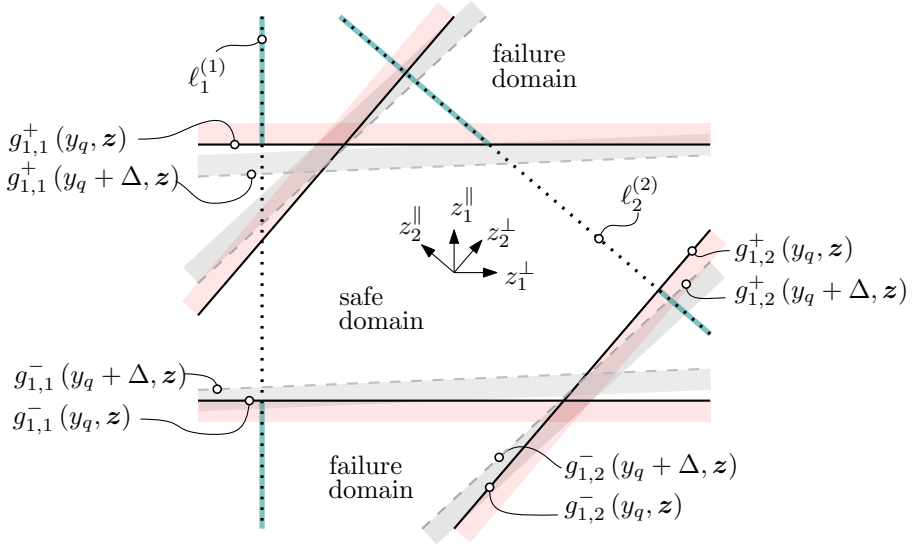

Figure 4: Effect of a design-parameter perturbation on the line-wise failure contribution.

Figure 4 shows the effect of a perturbation Δ of a design parameter y_q for the case $n_\eta = 1$ and $n_T = n_{KL} = 3$. The coordinate systems, weights, and importance sampling density are kept fixed for the design under consideration, so the explored line does not change. However, the perturbation from y_q to $y_q + \Delta$ modifies the elementary limit-state functions and shifts their intersections with the line. This changes the active safe-segment bounds and, consequently, the value of $A(\ell_j)$. This variation is finally reflected in the first excursion probability through Eq. (27). The derivatives of the active safe-segment bounds depend on the derivatives of the vectors $\boldsymbol{a}_{i,k}(\boldsymbol{y})$. Since these vectors are obtained from the dynamic response calculation, evaluating their derivatives requires differentiating the corresponding impulse response functions and spectral properties of the system [20].

Therefore, by approximating Eq. (27) with the same simulated lines used in Eq. (24), the sensitivity estimator by means of Importance Line Sampling is given by

$$\frac{\partial \tilde{p}_F}{\partial y_q} = \frac{\hat{p}_F}{N} \sum_{r=1}^{N} \frac{1}{A_{\Sigma}^{j_r}(\ell_{j_r,r})} \frac{\partial A(\ell_{j_r,r})}{\partial y_q}, \qquad q = 1, \ldots, n_Y. \tag{28}$$

Thus, the sensitivity estimate is obtained as a byproduct of the reliability analysis. The coefficient of variation of the sensitivity estimator is computed analogously to Eq. (25), using the sample variance of the weighted derivative contributions and the absolute value of $\partial \tilde{p}_F / \partial y_q$ in the normalization.

3.6 Implementation summary

The implementation of ILS follows directly from the quantities defined above and can be summarized as follows.

1. Compute $\boldsymbol{a}_{i,k}(\boldsymbol{y})$ from Eq. (5). Then evaluate $\boldsymbol{z}^*_{i,k}(\boldsymbol{y})$, $\beta_{i,k}$, $P[F_{i,k}]$, the directions $\boldsymbol{\alpha}_j$, the weights ρ_j, and the normalizing quantity $\hat{p}_F$.
2. For $r = 1, \ldots, N$:
   (a) Sample the coordinate-system index j_r according to ρ_j.
   (b) Sample $\boldsymbol{z}^{\perp}_{j_r,r}$ from $f^{\mathrm{IS},j_r}_{\boldsymbol{Z}^{\perp}_{j_r}}$ and define the explored line $\ell_{j_r,r}$.
   (c) Intersect $\ell_{j_r,r}$ with the elementary limit-state boundaries and determine c_S^{L,j_r} and c_S^{U,j_r}.
   (d) Evaluate $A(\ell_{j_r,r})$ and $A_{\Sigma}^{j_r}(\ell_{j_r,r})$ from Eqs. (17) and (21).
   (e) If sensitivities are required, keep the coordinate systems, weights, and importance sampling density fixed, and evaluate $\partial A(\ell_{j_r,r})/\partial y_q$ from the displacement of the active safe-segment bounds.
3. After N simulated lines, compute $\tilde{p}_F$ and $\delta_{\tilde{p}_F}$ from Eqs. (24) and (25). If sensitivities are required, compute $\partial \tilde{p}_F / \partial y_q$ from Eq. (28).

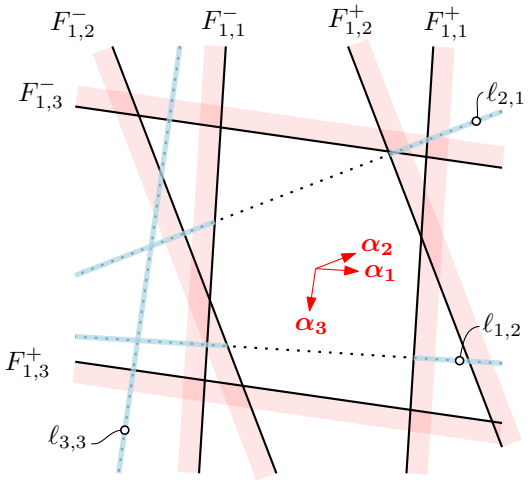

Figure 5: Representative explored lines in different coordinate systems during the ILS procedure.

Figure 5 illustrates the line-generation step of the ILS procedure for the case $n_\eta = 1$ and $n_T = n_{KL} = 3$. The three important directions $\boldsymbol{\alpha}_1$, $\boldsymbol{\alpha}_2$, and $\boldsymbol{\alpha}_3$ define the corresponding coordinate systems, and the representative lines $\ell_{2,1}$, $\ell_{1,2}$, and $\ell_{3,3}$ show how different realizations may be generated in different coordinate

systems during the simulation. Each explored line is parallel to the important direction of the selected coordinate system and is positioned by the sampled perpendicular realization. Its intersections with the elementary failure-domain boundaries are then used to determine the active safe segment and to evaluate the line-wise quantities required in the reliability and sensitivity estimators.

4 Numerical example: curved bridge model

The proposed approach is illustrated with a three-dimensional finite element model of a curved reinforced-concrete bridge subjected to stochastic ground excitation. The model contains 10068 degrees of freedom and is used to assess the performance of ILS in a large-scale setting. The bridge superstructure is modeled as a monolithic box girder and is curved in plan view, as illustrated in Figure 6. It has a total length of 119 m, divided into five spans of 24 m, 20 m, 23 m, 25 m, and 27 m. The substructure consists of four circular columns, denoted by $C_1, \ldots, C_4$, each with diameter 1.6 m and height 8 m. Each column is supported by four piles of length 35 m and diameter 0.6 m. The pile–soil interaction is represented by translational linear springs in the horizontal directions, whose stiffness varies linearly along the pile length from 112 MN/m at the deepest point to zero at the ground surface. All structural components are assumed to be made of reinforced concrete with Young's modulus $E = 2.0 \times 10^{10}$ N/m^2, Poisson's ratio $\nu = 0.2$, and mass density $\rho = 2500$ kg/m^3. The structure is modeled as linear elastic, and classical damping equal to 3% of critical damping is assigned to the first 100 retained modes.

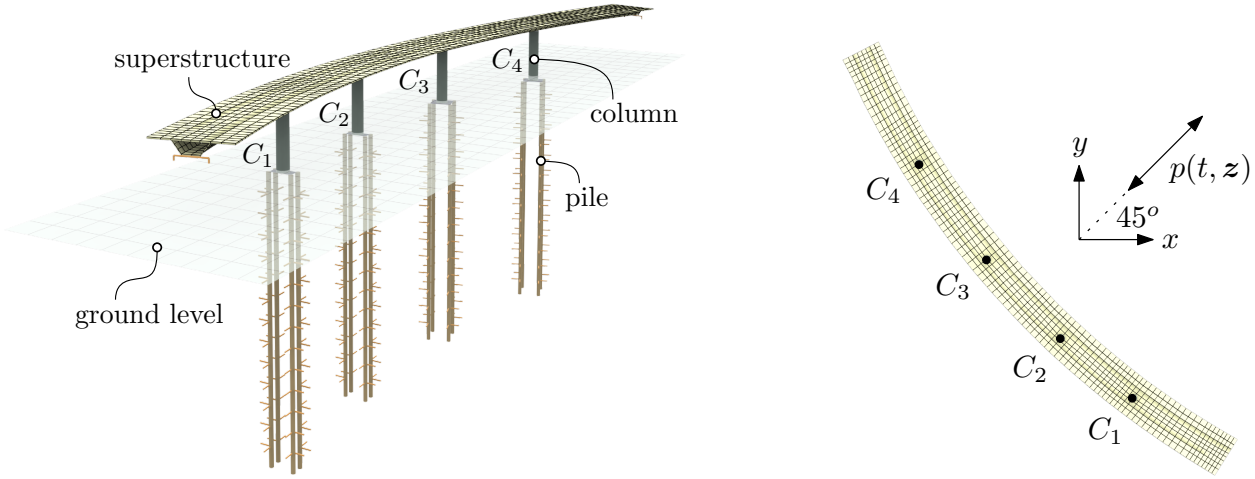

(a) Perspective view.

(b) Plan view.

Figure 6: Finite element model of the curved bridge.

The bridge is excited by a stochastic ground acceleration acting at an angle of 45° with respect to the global x axis. The excitation is modeled as a modulated and filtered Gaussian white-noise process. The underlying white-noise process has spectral intensity $S = 5 \times 10^{-4}$ m^2/s^3 and duration $T = 10$ s. The time step is $\Delta t = 0.01$ s, leading to $n_T = 1001$ analysis instants. All Karhunen–Loève terms are retained, so that $n_{KL} = 1001$. The white-noise process is passed through a Clough–Penzien filter, and the non-stationary character of the excitation is introduced through the deterministic modulation function (see Figure 7).

$$m(t) = \begin{cases} (t/5)^2, & 0 \le t \le 5 \text{ s}, \\ 1, & 5 \text{ s} < t \le 6 \text{ s}, \\ \exp\left[-(t-6)^2\right], & t > 6 \text{ s}. \end{cases} \tag{29}$$

The structure is assumed to be initially at rest. The first excursion event is defined in terms of the horizontal relative displacements between the bottom and top of each column, evaluated in the x and y directions. Therefore, two responses are considered per column, leading to $n_\eta = 8$ responses of interest. The prescribed

threshold is set to $b_i = 0.02$ m for all responses. Since the responses are evaluated at $n_T = 1001$ time instants, the failure domain is composed of $n_\eta n_T = 8008$ elementary failure domains. The deterministic design parameters considered in the sensitivity analysis are the diameters of the four bridge columns. Thus, y_q denotes the diameter of column C_q, with $q = 1, \ldots, 4$.

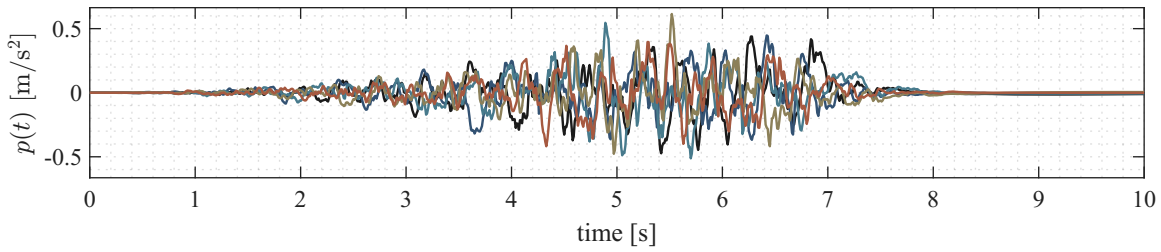

Figure 7: Five sample realizations of the stochastic ground acceleration.

The first excursion probability is estimated with ILS and compared with DDM, DIS, and mLS. The comparison is performed for a target coefficient of variation $\delta_{\tilde{p}_F} = 0.05$. Since DDM and DIS require one dynamic analysis per sample, whereas mLS and ILS require two, the computational effort is reported directly in terms of the number of dynamic analyses N_{dyn}. For mLS and ILS, the two analyses correspond to the evaluation of the response associated with the sampled perpendicular component and with the parallel direction used to construct the line-wise response. Figure 8 shows the evolution of the ILS estimate and its coefficient of variation, while Table 1 reports the final estimates, the number of dynamic analyses required to reach the prescribed precision, and the speed-up factor S_u with respect to ILS.

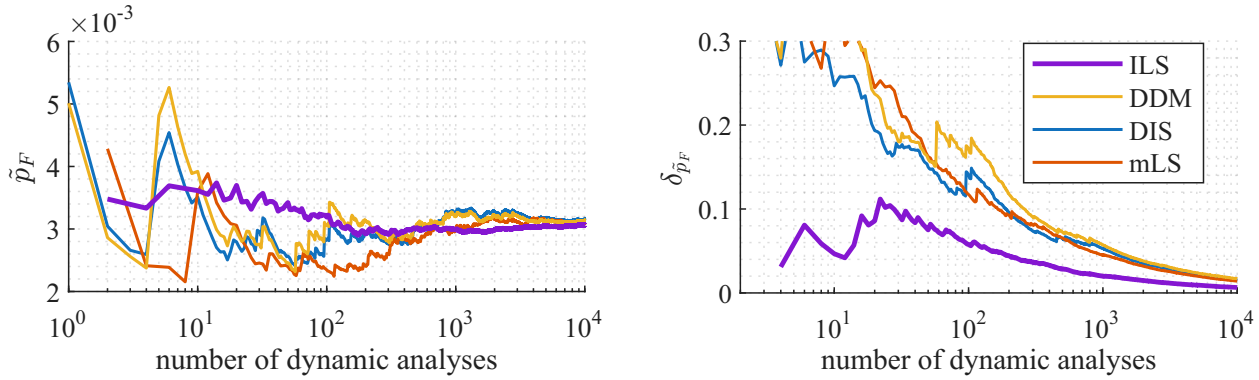

(a) Estimate of $\tilde{p}_F$.

(b) Coefficient of variation.

Figure 8: ILS versus DDM, DIS, and mLS: first excursion probability and coefficient of variation.

Table 1: First excursion probability estimates and computational effort for $\delta_{\tilde{p}_F} = 0.05$.

	ILS	DDM	DIS	mLS
$\tilde{p}_F$	3.059×10^{-3}	3.139×10^{-3}	3.157×10^{-3}	3.131×10^{-3}
N_{dyn}	154	1263	1099	800
S_u	1.00	8.20	7.14	5.19

All methods provide first excursion probability estimates close to 3.1×10^{-3}. However, ILS reaches the target coefficient of variation with the smallest number of dynamic analyses. In this example, DDM, DIS, and mLS require approximately 8.2, 7.1, and 5.2 times more dynamic analyses than ILS, respectively. This indicates that, for this example, the coordinate-system mixture and the associated line-wise importance density concentrate the sampling effort in relevant regions of the failure domain.

The sensitivity of the first excursion probability is then evaluated with respect to the four column diameters. Figure 9 shows the evolution of the ILS sensitivity estimates and their coefficients of variation. The final estimates are $\partial\tilde{p}_F/\partial y_1 = 3.545 \times 10^{-3}$, $\partial\tilde{p}_F/\partial y_2 = 3.422 \times 10^{-3}$, $\partial\tilde{p}_F/\partial y_3 = -8.017 \times 10^{-4}$, and $\partial\tilde{p}_F/\partial y_4 = -4.210 \times 10^{-3}$. The estimates associated with y_1 and y_2 are close to each other and therefore appear almost overlapped in the sensitivity plot. Both are positive, whereas the estimates associated with y_3 and y_4 are negative. Hence, increasing the diameters of columns C_1 and C_2 increases the first excursion probability, while increasing the diameters of columns C_3 and C_4 reduces it.

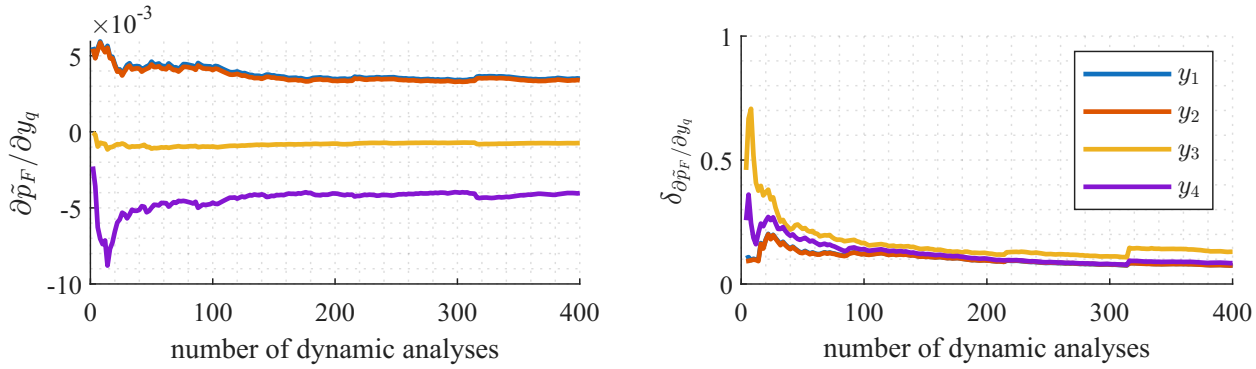

(a) Sensitivity estimates.

(b) Coefficients of variation.

Figure 9: ILS sensitivity estimates for the four column diameters and their coefficients of variation.

For a more detailed comparison with the reference methods, the sensitivity component associated with y_2 is considered. The target coefficient of variation is $\delta_{\partial\tilde{p}_F/\partial y_2} = 0.15$. Figure 10 shows the evolution of the ILS estimate of this component and its coefficient of variation, while Table 2 reports the final estimates and the number of dynamic analyses required by each method to reach the prescribed precision.

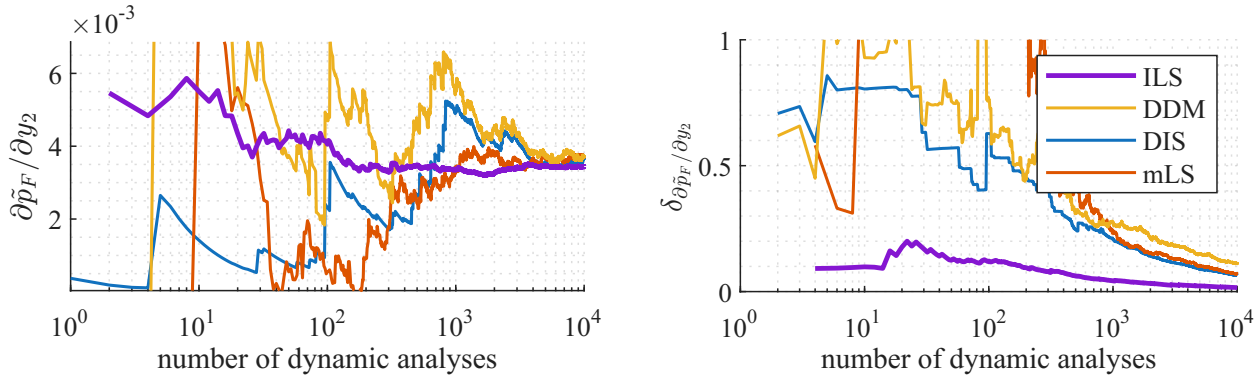

(a) Estimate of $\partial\tilde{p}_F/\partial y_2$.

(b) Coefficient of variation.

Figure 10: ILS versus DDM, DIS, and mLS: $\partial\tilde{p}_F/\partial y_2$ and coefficient of variation.

Table 2: Sensitivity estimates for y_2 and computational effort for $\delta_{\partial\tilde{p}_F/\partial y_2} = 0.15$.

	ILS	DDM	DIS	mLS
$\partial\tilde{p}_F/\partial y_2$	3.422×10^{-3}	3.715×10^{-3}	3.659×10^{-3}	3.697×10^{-3}
N_{dyn}	38	5950	1783	2456
S_u	1.00	156.58	46.92	64.63

The sensitivity estimates with respect to y_2 are of the same order for all methods. However, ILS reaches the prescribed coefficient of variation with a much smaller computational effort. The reduction is more

pronounced than in the probability estimation case, since the line-wise formulation captures the effect of the active intersections directly through the derivative of $A(\ell_j, \boldsymbol{y})$. This is consistent with the lower variability observed for the sensitivity estimator and with the larger speed-up obtained in the sensitivity analysis.

The signs of the sensitivity estimates can be interpreted from the curved geometry of the bridge and the observed dominant failure mechanism. In this example, the critical response is associated with the horizontal displacement of column C_4 in the x direction. Increasing the diameters of columns C_1 and C_2 stiffens the inner part of the bridge and modifies the plan-view deformation pattern. This tends to increase the displacement demand toward columns C_3 and C_4, and consequently increases the probability of exceeding the prescribed threshold. In contrast, increasing the diameters of columns C_3 and C_4 provides a more direct restraint of the dominant displacement response, reducing the first excursion probability. Therefore, the sensitivity estimates are not only numerical derivatives of the probability, but also provide useful information about how local stiffness modifications affect the global reliability of the curved bridge.

5 Conclusions and outlook

This work presented Importance Line Sampling for estimating the first excursion probability and its sensitivity in linear dynamical systems subject to Gaussian loading. The formulation exploits the linear dependence of the response on the Gaussian input variables, which allows the failure domain to be represented as a union of elementary linear failure domains. The corresponding design-point directions define multiple coordinate systems within a Line Sampling framework, and these coordinate systems determine the explored lines used for the analytical integrations. An importance sampling density is then introduced to concentrate the sampling effort in the relevant regions of the standard Gaussian space.

The proposed estimator evaluates the first excursion probability by analytical integration along the explored lines, while the sensitivity estimate is obtained as a byproduct of the reliability analysis from the derivative of the same line-wise contribution. In the curved bridge example, ILS provided accurate estimates of both quantities in a high-dimensional setting and achieved the prescribed precision with a markedly reduced number of dynamic analyses compared with DDM, DIS, and mLS. The improvement was particularly pronounced for the sensitivity estimate, where the proposed estimator substantially reduced the computational effort relative to the reference methods. These results suggest that the proposed method is particularly effective for large-scale dynamic reliability problems with a failure-domain structure similar to that observed in the bridge example, where the probability-relevant region is governed by a concentrated set of elementary failure domains.

Future developments will focus on how the elementary failure-domain structure affects the efficiency of ILS and on adaptive strategies for selecting the most informative coordinate systems. Further work will also consider importance sampling densities tailored to the sensitivity estimator. Finally, the application of ILS within reliability-based design optimization (RBDO) will be investigated, where repeated evaluations of the first excursion probability and its gradient are required.

Acknowledgements

Part of the research was funded by the State Key Laboratory of Disaster Reduction in Civil Engineering, Tongji University under project number SLDRCE24-02.

References

[1] T. Soong and M. Grigoriu, *Random Vibration of Mechanical and Structural Systems*. Englewood Cliffs, New Jersey: Prentice Hall, 1993.

[2] E. H. Vanmarcke, "On the distribution of the first-passage time for normal stationary random processes," *Journal of Applied Mechanics*, vol. 42, no. 1, pp. 215–220, 1975.

[3] H. Jensen and M. Valdebenito, "Reliability analysis of linear dynamical systems using approximate representations of performance functions," *Structural Safety*, vol. 29, no. 3, pp. 222–237, 2007.

[4] D. García, M. Rosales, and R. Sampaio, "Dynamic behaviour of a timber footbridge with uncertain material properties under a single deterministic walking load," *Structural Safety*, vol. 77, pp. 10–17, 2019.

[5] D. Honfi, A. Mårtensson, and S. Thelandersson, "Reliability of beams according to eurocodes in serviceability limit state," *Engineering Structures*, vol. 35, pp. 48–54, 2012.

[6] S. Au and J. Beck, "First excursion probabilities for linear systems by very efficient importance sampling," *Probabilistic Engineering Mechanics*, vol. 16, no. 3, pp. 193–207, 2001.

[7] L. Katafygiotis and S. Cheung, "Domain decomposition method for calculating the failure probability of linear dynamic systems subjected to Gaussian stochastic loads," *Journal of Engineering Mechanics*, vol. 132, no. 5, pp. 475–486, 2006.

[8] M. Misraji, M. Valdebenito, H. Jensen, and C. Mayorga, "Application of directional importance sampling for estimation of first excursion probabilities of linear structural systems subject to stochastic Gaussian loading," *Mechanical Systems and Signal Processing*, vol. 139, p. 106621, 2020.

[9] M. Valdebenito, P. Wei, J. Song, M. Beer, and M. Broggi, "Failure probability estimation of a class of series systems by multidomain Line Sampling," *Reliability Engineering & System Safety*, vol. 213, p. 107673, 2021.

[10] M. Friswell and J. Mottershead, "Finite element model updating in structural dynamics, kluwer academic publishers," 1995.

[11] G. Schuëller and H. Jensen, "Computational methods in optimization considering uncertainties – An Overview," *Computer Methods in Applied Mechanics and Engineering*, vol. 198, no. 1, pp. 2–13, 2008.

[12] A. Beck, W. Gomes, R. Lopez, and L. Miguel, "A comparison between robust and risk-based optimization under uncertainty," *Structural and Multidisciplinary Optimization*, vol. 52, no. 3, pp. 479–492, 2015.

[13] I. Papaioannou, K. Breitung, and D. Straub, "Reliability sensitivity estimation with sequential importance sampling," *Structural Safety*, vol. 75, pp. 24–34, 2018.

[14] M. A. Misraji, M. A. Valdebenito, and M. G. Faes, "First excursion probability sensitivity in stochastic linear dynamics by means of domain decomposition method," *Mechanical Systems and Signal Processing*, vol. 235, p. 112865, 2025.

[15] Z. Lu, S. Song, Z. Yue, and J. Wang, "Reliability sensitivity method by line sampling," *Structural Safety*, vol. 30, no. 6, pp. 517–532, 2008.

[16] M. Valdebenito, H. Jensen, H. Hernández, and L. Mehrez, "Sensitivity estimation of failure probability applying line sampling," *Reliability Engineering & System Safety*, vol. 171, pp. 99–111, 2018.

[17] A. Chopra, *Dynamics of structures: theory and applications to earthquake engineering*. Prentice Hall, 1995.

[18] A. Der Kiureghian, "The geometry of random vibrations and solutions by FORM and SORM," *Probabilistic Engineering Mechanics*, vol. 15, no. 1, pp. 81–90, 2000.

[19] P. Koutsourelakis, H. Pradlwarter, and G. Schuëller, "Reliability of structures in high dimensions, part I: Algorithms and applications," *Probabilistic Engineering Mechanics*, vol. 19, no. 4, pp. 409–417, 2004.

[20] I.-W. Lee and G.-H. Jung, "An efficient algebraic method for the computation of natural frequency and mode shape sensitivities - part I. distinct natural frequencies," *Computers & Structures*, vol. 62, no. 3, pp. 429–435, 1997.